− International Doctorate Program −

Identification, Optimization and Control with Applications in Modern Technologies

---

Kurt Chudej, Hans Josef Pesch, Kati Sternberg

Optimal Control of Load Changes for Molten Carbonate Fuel Cell Systems: A Challenge in PDE Constrained Optimization

April 23, 2009

Preprint IOC-25

Elite Network of Bavaria

OPTIMAL CONTROL OF LOAD CHANGES FOR MOLTEN CARBONATE FUEL CELL SYSTEMS: A CHALLENGE IN PDE CONSTRAINED OPTIMIZATION*

KURT CHUDEJ†, HANS JOSEF PESCH‡, AND KATI STERNBERG§

Abstract. Molten carbonate fuel cells provide a promising technology for the operation of future stationary power plants. In order to enhance service life, a detailed understanding of the dynamical behavior of such fuel cell systems is necessary. In particular, fast load changes shall be simulated, respectively optimized without risking material stress due to the extreme temperature differences usually accompanying fast load changes. Fast load changes are important for daily operations in order to react on varying demands. Material stress may lead to irreparable damage of the fuel cell stack.

For these contradicting goals, a family of hierarchically ordered mathematical models has been developed with the aim to simulate and optimize the temporal and spatial dynamical behavior of the gas streams, the chemical reactions, and the potential fields within the fuel cells. Altogether, the most complicated system, which is investigated in the present paper, results in a Pareto-optimal control problems with constraints in form of a huge system of 28 partial differential-algebraic (PDAE) and ordinary integro-differential-algebraic equations (OIDAE) and boundary conditions which are themselves partly given by an ordinary differential-algebraic system (ODE) of dimension 9. The partial differential equations (PDE) are of parabolic and hyperbolic type; some are degenerate. Moreover, the variables being involved in the different submodels of this fully coupled multi-physics system live on considerably different time scales.

Optimal control results are presented for a compromise between sufficiently fast load changes and sufficiently small temperature differences within the cell's solid part by means of a specially tailored formulation of a chain of optimal control problems. This procedure benefits from the different time scales of the state variables and keeps the problem manageable and computable despite its tremendous complexity and scale, although standard numerical methods are employed.

Key words. PDE constrained optimal control, partial differential-algebraic equations, molten carbonate fuel cells.

AMS subject classifications. 35M10, 34A09, 35K05, 35L80, 35Q80

1. Introduction.

Molten carbonate fuel cell systems (MCFC) are an efficient and environmentally friendly technology for the stationary simultaneous production of electrical energy and heat (resp. cooling) [26, 28].

MCFC belong to the class of high temperature fuel cells. The operation temperature is about 600 °C. In contrast to low temperature fuel cells, the temperature is high enough to allow internal reforming, i.e. the production of hydrogen from different kinds of fuel gases (e.g. methane) internally in the cell system. Moreover, neither expensive catalysts nor expensive ceramics are needed for an efficient operation. Due to the high operating temperatures, it is, however, difficult to operate MCFC. Because one has to observe a certain range of admissible temperatures. For chemical and electrochemical reactions decelerate in regions of low temperature, whereas catalysts degrade quickly in regions of high temperature. In addition, spatial temperature dif-

*This work was funded from 2002 to 2005 by the German Federal Ministry of Education and Research (BMBF) within the project *Optimierte Prozessführung von Brennstoffzellensystemen mit Methoden der Nichtlinearen Dynamik*. Kati Sternberg was supported in 2006 by the *Promotionsabschlussstipendium* of the HWP-Programme *Chancengleichheit für Frauen in Forschung und Lehre*.

†Universität Bayreuth, Lehrstuhl für Ingenieurmathematik, 95440 Bayreuth, Germany (Corresponding author: kurt.chudej@uni-bayreuth.de).

‡Universität Bayreuth, Lehrstuhl für Ingenieurmathematik, 95440 Bayreuth, Germany

§Merz Pharmaceuticals GmbH, Frankfurt, Germany; formerly: Universität Bayreuth, Lehrstuhl für Ingenieurmathematik, 95440 Bayreuth, Germany

ferences have to be moderate to avoid material corrosion due to temperature induced stresses. Therefore, the cell temperatures are crucial for the system's performance and lifetime.

MCFC systems have been and are being developed and tested by several companies around the world and can be expected to become competitive to classical power plants within the next few years [2, 18, 22]. However, further efforts are still necessary to increase their efficiency, to develop better control strategies, and to improve their long time stability. Besides experimental validations, mathematical models are an indispensable tool to achieve these goals. Potentially dangerous or even disastrous control scenarios for real stacks of fuel cells can be safely simulated by means of mathematical models. Realistic mathematical models [11, 13, 17] based on physical and chemical laws have paved the road to apply mathematical optimization and optimal control techniques. Moreover mathematical models allow to study different designs in advance such as crossflow versus counterflow guidance of the gas streams [23] or different (optimal) catalyst distributions [15].

A general description of different fuel cell types can be found in [28], recent results on molten carbonate fuel cells in [26]. The mathematical models presented in the latter are part of a hierarchically ordered family of models. The most complicated of these models is investigated in the present paper. It has been taken from [11] and [17] where a detailed physical and chemical derivation of this and the other related models can be found: There exist models for 1D counterflow [4, 5, 12] and 2D crossflow configurations, models with or without consideration of the compartment pores in the anode and cathode gas channels, models with simplified chemical reactions neglecting the carbon monoxide fraction, models with or without a cathode gas recycle, particularly tailored models for special engineering purposes [14] or for the design of a state estimator based on reduced models by means of proper orthogonal decomposition techniques [9]. This state estimator has been used for the practical operation of the MCFC in the power plant of the University Hospital of Magdeburg operated by the IPF-Heizkraftwerksbetriebsgesellschaft mbH Magdeburg [19]. This MCFC of type *HotModule* was produced by the MTU CFC Solutions GmbH Munich [18]. A further model variant, which has been validated [10] on the *HotModule*, includes indirect internal reforming [17].

Concerning appropriate mathematical methods for the simulation and optimization of the different model variants, the authors have investigated the indices of the model equations (differential time index [5, 6, 24], perturbation index [6, 23]), which proves the well-posedness of the equations, and have performed numerical simulations [7]. They also have computed optimal controls [24] and have carried through a numerical sensitivity analysis of the resulting optimal solutions [25] for regular operations as well as for fast load changes.

This article is based on the third author's PhD thesis [23] and presents, for the first time, optimal control results, which take into account more strictly the two contradicting engineering objectives: fast load changes as well as limited differences of the solid temperature.

The following issues are typical in an interdisciplinary project of engineers and mathematicians who tackle conjointly an industrial real-life problem: The models to be investigated may have considerably high complexity and may be, in addition, frequently modified and adapted during the course of the project. This obviously has consequences for the choice of appropriate numerical methods which usually have to be developed in parallel to the development of the models to enable immediate feedback

to the modelers. The numerical methods must therefore be easily manageable, in particular with respect to model changes.

Additional challenges are posed by the coupling of different types of equations due to the generally multi-physics character of real-life applications. Therefore (special) finite difference (volume) schemes have been chosen as a unified approach for the numerical treatment of the different kinds of differential equations versus (special) finite element methods, respectively (discontinuous) Galerkin methods. Our approach may not be efficient with respect to computing time but it seems to be efficient with respect to man-machine communication during the simultaneous development of the complicated family of models, on which we report here and which took over about three years. We will come back to this point later.

Additionally, the aim of the paper is to present a complete model for an interesting, important and challenging application in engineering sciences to encourage further investigations with respect to its theoretical analysis and to more efficient numerical methods. The problem may provide a challenging benchmark for (optimal) control and sensitivity analysis of PDE constrained optimization problems, a topic of currently high research endeavors.

2. The 2D molten carbonate fuel cell model. The mathematical model of Heidebrecht [11], see also [17, 23], which is investigated in the present paper, describes an averaged single MCFC of a stack of about 350 cells. The model is based on physical and chemical laws for the gas transport and the electro-chemical reactions which take place in each single fuel cell. The underlying design is a crossflow configuration with respect to the anode and cathode gas flows; see Fig. 2.1. This figure shows a 3D view of the compartments of the anode and cathode gas channels, the solid/electrolyte, the catalytic burner and mixer, and the configuration of the gas flows.

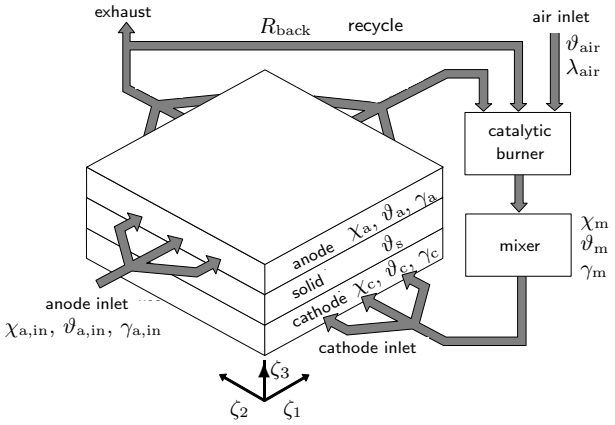

FIG. 2.1. *Crossflow model of a MCFC with compartments and mathematical variables*

In the anode/cathode compartments, the fuel gas actually flows through several small pipes parallel to the ζ_1-axis, respectively ζ_2-axis. Since the cell is sufficiently flat the third dimension ζ_3 can be neglected. Such a design has been realized for the *HotModule* mentioned above.

We cite the most important model assumptions from [11, 17] where more technical details can be found: First, plug flow conditions for the gas phase in anode and cathode are assumed, where different phases may have different temperatures

and may exchange heat. All solid parts of the cell are lumped to one phase with respect to the enthalpy balance. The temperatures of the two gas phases are calculated separately, and the MCFC is operated at nearly ambient pressure. We do not consider pressure drops across the gas channels, i.e., isobaric conditions are assumed. All cells in the stack behave alike, so that the simulation of a single cell is sufficient when taking symmetry conditions at boundaries of neighboring cells into account. All chemical substances have the same heat capacity, which is assumed to be independent of the temperature. Reaction enthalpies are also assumed to be independent of the temperature. The temperature dependent chemical equilibrium constants and standard open circuit voltages are approximated by affine-linear functions. Ideal gas law is applied. The reforming reactions in the anode gas channel are modeled as quasi-homogeneous gas phase reactions using volume-related reaction rates. Methane steam reforming and water gas shift reactions are considered. Their heat of reaction is fully transferred to the gas phase. Diffusion in flow direction is negligible compared to convective transport. Heat exchange between electrode and gas phase is described by a linear function. The corresponding heat exchange coefficient also includes the effect of thermal radiation in linearized form.

The more detailed Fig. 2.2 additionally depicts the variables in the pores and the considered chemical reactions: the reforming reactions (ref1, 2) take place in the anode gas channel, the oxidation reactions (ox1, 2) in the pores of the anode, the reduction reaction in the pores of the cathode.

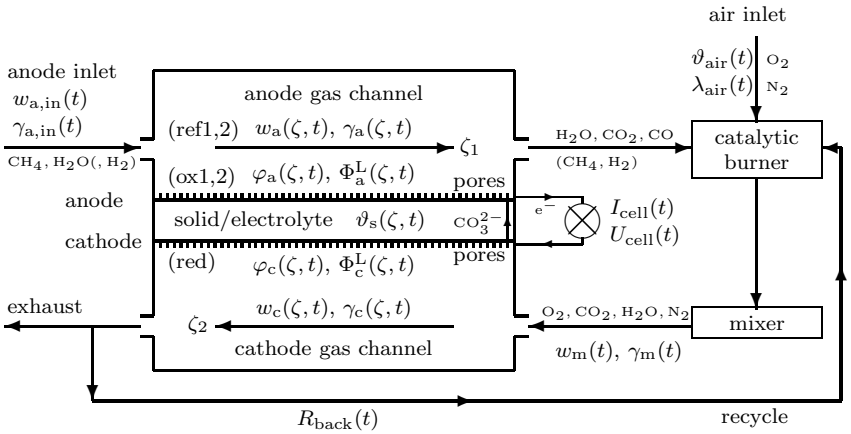

(ref1) $CH_4 + H_2O \rightleftharpoons CO + 3\,H_2$ (ref2) $CO + H_2O \rightleftharpoons CO_2 + H_2$

(ox1) $H_2 + CO_3^{2-} \rightleftharpoons H_2O + CO_2 + 2e^-$ (ox2) $CO + CO_3^{2-} \rightleftharpoons 2\,CO_2 + 2e^-$

(red) $\frac{1}{2}O_2 + CO_2 + 2e^- \rightleftharpoons CO_3^{2-}$

FIG. 2.2. *2D crossflow model of a molten carbonate fuel cell with variables* $w := (\chi, \vartheta)$, χ = vector of molar fractions, ϑ = temperature, φ = vector of partial pressures, γ = molar flow density, Φ = electrical potentials, U_{cell} = cell voltage, I_{cell} = cell current

The compartments of the cell are denoted by an index k: a = anode gas channel/anode pores, c = cathode gas channel/cathode pores, s = solid, e = electrolyte, m = mixer, in = inlet, out = outlet. The seven gas components are denoted by the index set $\mathcal{I} := \{CH_4, H_2O, H_2, CO, CO_2, O_2, N_2\}$ and are used for the molar fractions $\chi_{j,k}$ and the partial pressures $\varphi_{j,k}$, $j \in \mathcal{I}$, $k \in \{\mathrm{a}, \mathrm{c}, \mathrm{m}\}$. Note that the (non-

negative) molar fractions sum up to 1 in each of the compartments k. Furthermore, we have to take into account the molar flow densities γ_k as well as the gas temperatures ϑ_k, $k \in \{\mathrm{a}, \mathrm{c}, \mathrm{m}\}$.

The gas temperatures ϑ_a and ϑ_c are dominated by convection and have to be distinguished from the solid temperature ϑ_s which is distributed by heat conduction. $1 - R_\mathrm{back}(t)$ denotes the fraction of the gas stream from the anode gas outlet which goes to the exhaust.

The electric potential, which is spatially distributed in the MCFC, is essential for the dynamical behavior. Its associated submodel is based on the spatially 1D version of Poisson's law and discrete charge layers. We assume spatially constant electric potentials at the electrodes, transport of the carbonate ions orthogonal to the ζ_1-ζ_2-plane and transient charge balances. The electrical potentials $\Phi_\mathrm{a}^\mathrm{L}$, $\Phi_\mathrm{c}^\mathrm{L}$, and the voltage U_cell are defined relatively to a reference potential $\Phi_\mathrm{a}^\mathrm{s} = 0$. Additionally, we have to take into account the current densities i_k as well as the currents I_k, $k \in \{\mathrm{a}, \mathrm{c}, \mathrm{e}\}$, in the electrolyte; see Fig. 2.3.

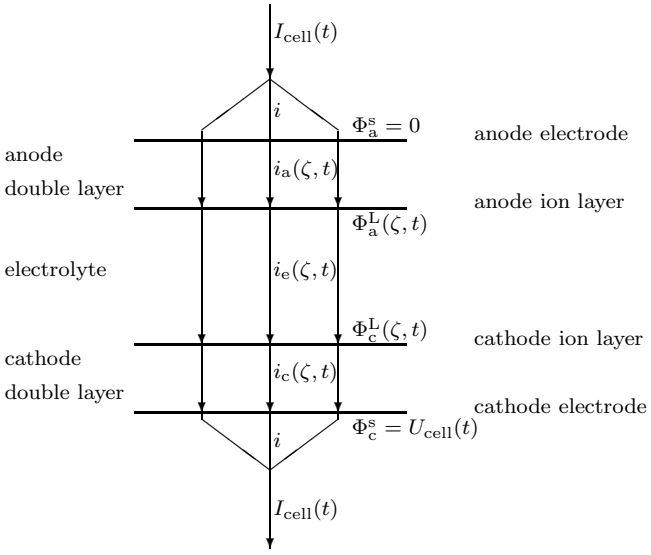

FIG. 2.3. *Electric potential field model*

The total cell current $I_\mathrm{cell}(t)$ shall be prescribed either by a constant function or a piecewise constant step function. Finally, the following vectors are introduced: $w_k := (\chi_k, \vartheta_k)$, $w_{\mathrm{a|c}} := (w_\mathrm{a}, w_\mathrm{c})$, $\varphi_{\mathrm{a|c}} := (\varphi_\mathrm{a}, \varphi_\mathrm{c})$, $\Phi_{\mathrm{a|c}}^\mathrm{L} := (\Phi_\mathrm{a}^\mathrm{L}, \Phi_\mathrm{c}^\mathrm{L})$.

Altogether, we end up with a system of time dependent nonlinear partial differential algebraic equations in the two spatial coordinates $\zeta := (\zeta_1, \zeta_2) \in \Omega := (0,1) \times (0,1)$. The boundary of Ω is denoted by $\partial\Omega$.

All variables are dimensionless. One unit of the dimensionless time t equals 12.5 [sec]. A single fuel cell is of a rectangular size of about 1.2 [m] by 0.8 [m]. One unit of the dimensionless temperature ϑ equals 298.15 [K]. One unit of the dimensionless molar flow density γ equals 6.377 [m mol/sec].

2.1. Mathematical model equations. The model consists, due to its multiphysics character, of the following submodels:

1. The PDAE system with boundary conditions for the cell's dynamic:

$$c_{\mathrm{p,s}}\,\frac{\partial \vartheta_{\mathrm{s}}}{\partial t} = \kappa_1\,\frac{\partial^2 \vartheta_{\mathrm{s}}}{\partial \zeta_1^2} + \kappa_2\,\frac{\partial^2 \vartheta_{\mathrm{s}}}{\partial \zeta_2^2} + \psi_1(\vartheta_{\mathrm{s}}, w_{\mathrm{a|c}}, \varphi_{\mathrm{a|c}}, \Phi^{\mathrm{L}}_{\mathrm{a|c}}, U_{\mathrm{cell}})\,, \tag{2.1}$$

$$\frac{\partial \vartheta_{\mathrm{s}}}{\partial n}\Big|_{\partial\Omega} = 0\,,$$

$$\frac{\partial w_{\mathrm{a}}}{\partial t} = -\,\gamma_{\mathrm{a}}\,\vartheta_{\mathrm{a}}\,\frac{\partial w_{\mathrm{a}}}{\partial \zeta_1} + \psi_2(\vartheta_{\mathrm{s}}, w_{\mathrm{a}}, \varphi_{\mathrm{a}}, \Phi^{\mathrm{L}}_{\mathrm{a}})\,, \tag{2.2}$$

$$w_{\mathrm{a}}|_{\partial\Omega_{\mathrm{a,in}}} = w_{\mathrm{a,in}}(t)\,,$$

$$\frac{\partial w_{\mathrm{c}}}{\partial t} = -\,\gamma_{\mathrm{c}}\,\vartheta_{\mathrm{c}}\,\frac{\partial w_{\mathrm{c}}}{\partial \zeta_2} + \psi_3(\vartheta_{\mathrm{s}}, w_{\mathrm{c}}, \varphi_{\mathrm{c}}, \Phi^{\mathrm{L}}_{\mathrm{c}}, U_{\mathrm{cell}})\,, \tag{2.3}$$

$$w_{\mathrm{c}}|_{\partial\Omega_{\mathrm{c,in}}} = w_{\mathrm{m}}(t)\,,$$

$$0 = -\,\frac{\partial(\gamma_{\mathrm{a}}\,\vartheta_{\mathrm{a}})}{\partial \zeta_1} + \psi_4(\vartheta_{\mathrm{s}}, w_{\mathrm{a}}, \varphi_{\mathrm{a}}, \Phi^{\mathrm{L}}_{\mathrm{a}})\,, \tag{2.4}$$

$$\gamma_{\mathrm{a}}|_{\partial\Omega_{\mathrm{a,in}}} = \gamma_{\mathrm{a,in}}(t)\,,$$

$$0 = -\,\frac{\partial(\gamma_{\mathrm{c}}\,\vartheta_{\mathrm{c}})}{\partial \zeta_2} + \psi_5(\vartheta_{\mathrm{s}}, w_{\mathrm{c}}, \varphi_{\mathrm{c}}, \Phi^{\mathrm{L}}_{\mathrm{c}}, U_{\mathrm{cell}})\,, \tag{2.5}$$

$$\gamma_{\mathrm{c}}|_{\partial\Omega_{\mathrm{c,in}}} = \gamma_{\mathrm{m}}(t)\,,$$

$$0 = \psi_6(\vartheta_{\mathrm{s}}, \chi_{\mathrm{a}}, \varphi_{\mathrm{a}}, \Phi^{\mathrm{L}}_{\mathrm{a}})\,, \qquad 0 = \psi_7(\vartheta_{\mathrm{s}}, \chi_{\mathrm{c}}, \varphi_{\mathrm{c}}, \Phi^{\mathrm{L}}_{\mathrm{c}}, U_{\mathrm{cell}})\,, \tag{2.6}$$

$$\frac{\partial \Phi^{\mathrm{L}}_{\mathrm{a}}}{\partial t} = \frac{i_{\mathrm{a}} - i}{c_{\mathrm{a}}}\,, \qquad \frac{\partial \Phi^{\mathrm{L}}_{\mathrm{c}}}{\partial t} = \frac{i_{\mathrm{a}} - i}{c_{\mathrm{a}}} + \frac{i_{\mathrm{e}} - i}{c_{\mathrm{e}}}\,. \tag{2.7}$$

2. The system of OIDAE for voltage and currents:

$$\frac{\mathrm{d}U_{\mathrm{cell}}}{\mathrm{d}t} = \frac{I_{\mathrm{a}} - I_{\mathrm{cell}}}{c_{\mathrm{a}}} + \frac{I_{\mathrm{e}} - I_{\mathrm{cell}}}{c_{\mathrm{e}}} + \frac{I_{\mathrm{c}} - I_{\mathrm{cell}}}{c_{\mathrm{c}}}\,, \tag{2.8}$$

$$I_{\mathrm{a}}(t) = \int_\Omega i_{\mathrm{a}}(\vartheta_{\mathrm{s}}, w_{\mathrm{a}}, \varphi_{\mathrm{a}}, \Phi^{\mathrm{L}}_{\mathrm{a}})\,\mathrm{d}\zeta\,, \tag{2.9}$$

$$I_{\mathrm{c}}(t) = \int_\Omega i_{\mathrm{c}}(\vartheta_{\mathrm{s}}, w_{\mathrm{c}}, \varphi_{\mathrm{c}}, \Phi^{\mathrm{L}}_{\mathrm{c}}, U_{\mathrm{cell}})\,\mathrm{d}\zeta\,, \tag{2.10}$$

$$I_{\mathrm{e}}(t) = \int_\Omega i_{\mathrm{e}}(\Phi^{\mathrm{L}}_{\mathrm{a|c}})\,\mathrm{d}\zeta\,, \tag{2.11}$$

$$i = \left(c_{\mathrm{a}}^{-1} + c_{\mathrm{e}}^{-1} + c_{\mathrm{c}}^{-1}\right)^{-1}\left(\frac{i_{\mathrm{a}} - I_{\mathrm{a}}}{c_{\mathrm{a}}} + \frac{i_{\mathrm{e}} - I_{\mathrm{e}}}{c_{\mathrm{e}}} + \frac{i_{\mathrm{c}} - I_{\mathrm{c}}}{c_{\mathrm{c}}}\right) + I_{\mathrm{cell}}\,. \tag{2.12}$$

3. The system of DAE for the coupling of anode outlet to cathode inlet:

$$\frac{dw_{\mathrm{m}}}{dt} = \psi_8(w_{\mathrm{m}}, \int_{\partial\Omega_{\mathrm{a,out}}} w_{\mathrm{a}}\,\mathrm{d}\zeta_2,\ \int_{\partial\Omega_{\mathrm{a,out}}} \gamma_{\mathrm{a}}\,\mathrm{d}\zeta_2,\ \int_{\partial\Omega_{\mathrm{c,out}}} w_{\mathrm{c}}\,\mathrm{d}\zeta_1, \int_{\partial\Omega_{\mathrm{c,out}}} \gamma_{\mathrm{c}}\,\mathrm{d}\zeta_1,\ \lambda_{\mathrm{air}},\ \vartheta_{\mathrm{air}},\ R_{\mathrm{back}})\,, \tag{2.13}$$

$$\gamma_{\mathrm{m}}(t) = \psi_9(w_{\mathrm{m}}, \int_{\partial\Omega_{\mathrm{a,out}}} w_{\mathrm{a}}\,\mathrm{d}\zeta_2,\ \int_{\partial\Omega_{\mathrm{a,out}}} \gamma_{\mathrm{a}}\,\mathrm{d}\zeta_2,\ \int_{\partial\Omega_{\mathrm{c,out}}} w_{\mathrm{c}}\,\mathrm{d}\zeta_1, \int_{\partial\Omega_{\mathrm{c,out}}} \gamma_{\mathrm{c}}\,\mathrm{d}\zeta_1,\ \lambda_{\mathrm{air}},\ \vartheta_{\mathrm{air}},\ R_{\mathrm{back}})\,. \tag{2.14}$$

4. Initial conditions:

$$\begin{aligned} \vartheta_{\mathrm{s}}|_{t=0} = \vartheta_{0,\mathrm{s}}(\zeta)\,,\ w_{\mathrm{a}}|_{t=0} = w_{0,\mathrm{a}}(\zeta)\,,\ w_{\mathrm{c}}|_{t=0} = w_{0,\mathrm{c}}(\zeta)\,,\ w_{\mathrm{m}}|_{t=0} = w_{0,\mathrm{m}}\,,\\ \Phi^{\mathrm{L}}_{\mathrm{a}}|_{t=0} = \Phi^{\mathrm{L}}_{0,\mathrm{a}}(\zeta)\,,\ \Phi^{\mathrm{L}}_{\mathrm{c}}|_{t=0} = \Phi^{\mathrm{L}}_{0,\mathrm{c}}(\zeta)\,,\ U_{\mathrm{cell}}|_{t=0} = U_{0,\mathrm{cell}}\,. \end{aligned} \tag{2.15}$$

The whole PDAE system is non-linear and of dimension 28. It consists, firstly, of a parabolic heat equation (2.1), secondly, of a system of 16 hyperbolic equations (2.2–2.3) for the reactive gas transport with fixed wind direction, because $\gamma_{\mathrm{a|c}}$ and $\vartheta_{\mathrm{a|c}}$ are positive, thirdly, of a system of 2 degenerate partial differential equations for the molar flow densities (2.4–2.5), fourthly, 2 algebraic equation systems for the reactions in the pores (2.6), fifthly, of a system of 2 ordinary differential equations in time for the (spatially dependent) potentials (2.7), and sixthly, of a system of 5 integro-differential-algebraic equations for voltage and currents (2.8–2.12). The system (2.13–2.14) of ordinary integro-differential-algebraic equations of dimension 9 is part of the boundary conditions in (2.1–2.5) and couples anode outlet with cathode inlet via catalytic burner and mixer. The initial-boundary-value problem is completed by the initial conditions (2.15).

To keep the notation compact here, the functions $\psi_\diamond$ as well as $i_{a|c|e}$ and all data can be found in the appendix.

For numerical simulations, the boundary functions $w_{\mathrm{a,in}}(t)$, $\gamma_{\mathrm{a,in}}(t)$ at the anode gas inlet in (2.2, 2.4), and the functions $\lambda_{\mathrm{air}}(t)$, $\vartheta_{\mathrm{air}}(t)$, $R_{\mathrm{back}}(t)$ in (2.13, 2.14) at the air inlet are prescribed. Some of these quantities will later be used for control purposes. The cell current $I_{\mathrm{cell}}(t)$ is also an input, but not a control variable and will later be used to simulate prescribed load changes.

2.2. Local existence and uniqueness. Existence and uniqueness results for the complete initial-boundary-value problem are still open. However, local existence results (in time) can be proven for each of the submodels by standard arguments if all quantities not governed by the associated subsystem are assumed to be given suitable sufficiently smooth time dependent functions. For more details, see [23].

2.3. Index analysis and numerical discretization. A detailed index analysis of (2.1–2.12) yields the differential time index $\nu_t = 1$ (see [24]; some small modifications have to be made therein: the cathode recycle has been turned off). These investigations yield the consistent initial conditions (2.15). Note that no initial conditions can be prescribed for the algebraic variables $\gamma_{\mathrm{a|c|m}}$, $\varphi_{\mathrm{a|c}}$, and $I_{\mathrm{a|c|e}}$.

An appropriate numerical method is the vertical method of lines (MOL), which is based on a semi-discretization in space. This is alleviated by the a priori known wind

direction of the hyperbolic equations. A five-point star for the (scaled) Laplacian and suitable conservative upwind formulas are used for the spatial derivatives of the transport equations as well as order-preserving quadrature formulas for the spatial integrals; see [23]. Here, the property of the molar fractions, which sum up to 1 in each of the compartments, is an excellent indicator for an appropriate conservative discretization.

All in all, this yields a very large semi-explicit system of (ordinary) differential--algebraic equations (DAE) in time of dimension $25\,N^2 + 6$, where N denotes the number of spatial grid points in one spatial direction. This system has index $\nu = 1$ and is of the form

$$M\dot{x}(t) = g(x(t), u(t))\,, \qquad M[x(0) - x_0] = 0\,, \qquad M = \mathrm{diag}(I, O)\,. \tag{2.16}$$

3. Steady state solution. The numerical procedure to determine a steady state solution of (2.16) for a given constant cell current is intricate, and mimics somehow the starting procedure for a real fuel cell.

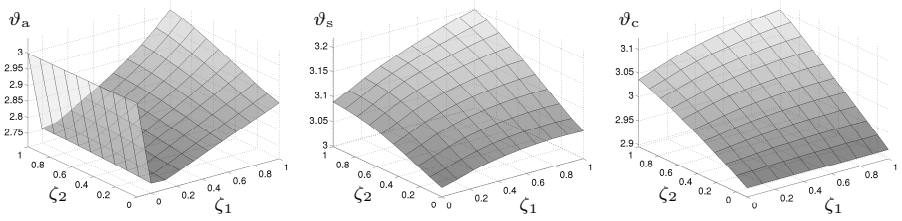

(a) Anode gas temperature (b) Solid temperature (c) Cathode gas temperature

FIG. 3.1. *Temperatures (steady state)*

The difficulties are caused by the unknown initial conditions of the DAE. The procedure consists of firstly solving only certain equations and then adapting boundary conditions and model constants during the time integration step-by-step. A detailed description of this rather technical approach would be beyond the scope of the paper. For more details, see [23]. The run time for a steady state solution from the scratch for a 10×10 spatial discretization takes about 1 day on a 1.8 GHz PC. Supercomputers have been consciously not used to meet the usual industrial requirements. The obtained steady state solution is then stored and used as initial condition for the optimization.

TABLE 3.1
Constant boundary and input data for the steady state solution

anode gas inlet		air inlet		exhaust feedback	
$\chi_{CH_4,a,in}$	2/7	λ_{air}	2.2	R_{back}	0.5
$\chi_{H_2O,a,in}$	5/7	ϑ_{air}	1.5		
$\vartheta_{a,in}$	3.0			cell current	
$\gamma_{a,in}$	1.0			I_{cell}	0.7

The resulting steady state solution is shown in Figs. 3.1–3.4; see Table 3.1 for the data used.

Note that a comparable steady state solution has been independently computed by our project partners; it can be found in [11]. Different software packages have

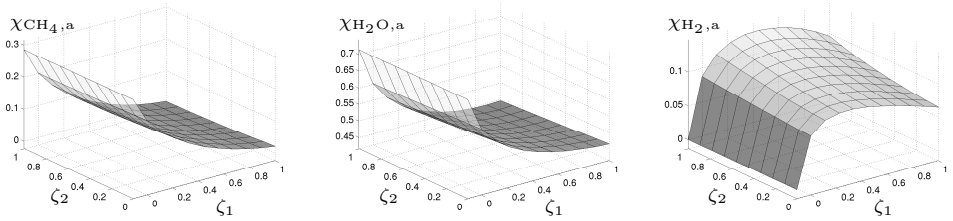

FIG. 3.2. *Molar fractions in the anode gas channel (steady state)*

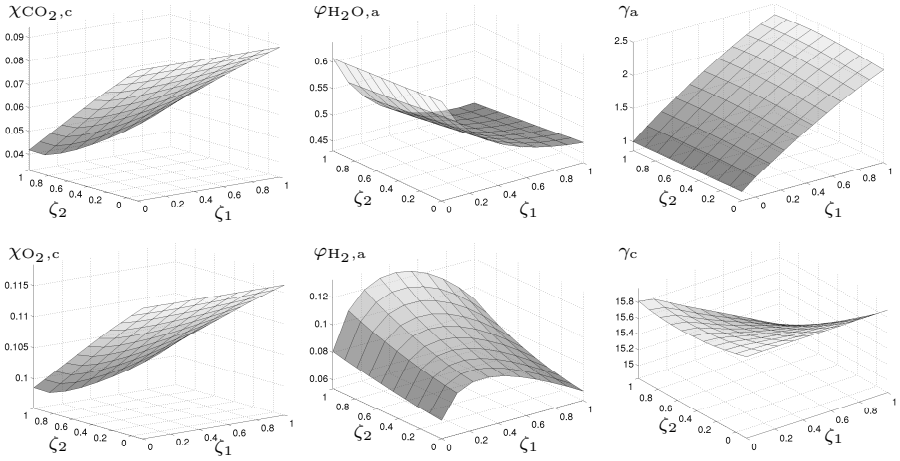

(a) Molar fractions in the cathode gas channel (b) Partial pressures in anode pores (c) Molar flow densities

FIG. 3.3. *Molar fractions in the cathode gas channel (left), partial pressures in anode pores (middle), molar flow densities (right); steady state*

been used there: ProMoT [27] and DIVA [20]. The comparison indicates a correct implementation of the whole model within numerical accuracy.

The solid temperature ϑ_s is the most important quantity of the MCFC model. It describes the temperature distribution in the solid parts, especially in the porous matrix which is filled by the electrolyte. Figure 3.1 (b) depicts the steady state solution of ϑ_s. Figures 3.1 (a) and 3.1 (c) show the temperature distribution in the anode and cathode gas channels as well as the boundary data at their inlets.

The solid temperature ϑ_s depends on the gas temperatures $\vartheta_{a|c}$ and the exothermic and endothermic reactions. Note that the reaction rates r_j depend on temperatures, see appendix. For example, the solid temperature is maximal with $\vartheta_s(1,1) = 3.199 \mathrel{\widehat{=}} 954$ [K] at the corner $(\zeta_1 = 1, \zeta_2 = 1)$ because of the high anode and cathode gas temperatures there; see Figs. 3.1. Analogously, the solid temperature is minimal with $\vartheta_s(0,0) = 3.017 \mathrel{\widehat{=}} 900$ [K] at the corner $(\zeta_1 = 0, \zeta_2 = 0)$. In the other two corners, the solid temperature ϑ_s is moderate, since only one of the two gas temperatures $\vartheta_{a|c}$ is high. Note that the feed gas at the anode inlet is already pre-heated.

The anode gas temperature ϑ_a is firstly decreasing in flow direction ζ_1, because the reforming reactions (ref1,2) are endothermic altogether. The produced hydrogen H_2 is then used in the exothermic oxidation (ox1,2) in the pores. Therefore, the anode gas temperature ϑ_a is increasing further downwards. In the catalytic burner, the remaining molar fractions of hydrogen, methane CH_4, and carbon monoxide CO are

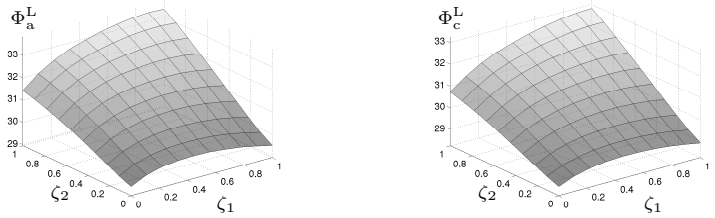

FIG. 3.4. *Electrical potentials (steady state)*

burnt up. Therefore, the temperature at the cathode inlet exceeds that of the anode outlet. In the cathode gas channel, the gas temperature ϑ_c then increases with flow direction ζ_2 due to the exothermic reduction reaction.

The molar fractions and partial pressures of the gas components are a result of the gas flows and the five chemical reactions. Figures 3.2 and 3.3 show selected molar fractions and partial pressures in the anode and cathode gas channel, and the molar flow densities. Figure 3.2 shows the decrease of methane and water H_2O as hydrogen is produced in the anode gas channel. Further downward in flow direction ζ_1, the hydrogen itself decreases due to the electrochemical oxidation. Figure 3.3(a) depicts the decrease of oxygen O_2 and carbon dioxide CO_2 in flow direction ζ_2 of the cathode gas channel due to the reduction reaction (red). The produced carbonate ions are transferred from the cathode electrode through the electrolyte to the anode electrode. Then they are used for the oxidation reaction (ox1,2). Methane, hydrogen, and carbon monoxide can be neglected in the cathode gas channel, since they have been burnt up in the catalytic burner as mentioned before. Figure 3.3(c) presents the molar flow densities. The electrical potentials Φ_a^L and Φ_c^L (Fig. 3.4) are correlated with the high reaction rates of (ox1,ref) and thus with a high solid temperature ϑ_s; cf. Fig. 3.1(b).

The output parameters for the steady state are given in Table 3.2; see [17] and [23] for more details.

TABLE 3.2
Output parameters (steady state)

cell voltage U_{cell}	$29.773 \mathrel{\widehat{=}} 0.765$ V
cell power P_{cell}	$47.638 \mathrel{\widehat{=}} 0.753$ kW
electrical efficiency η_{el}	0.497

4. Optimal control of fast load changes. A (possibly discontinuous) change in the input function $I_{\text{cell}}(t)$, typically a piecewise constant function, is called load change. The ability of performing fast load changes is important for the operation of power plants to react on varying demand. After a load change, the new steady state should be reached as soon as possible, while large spatial differences of the solid temperature simultaneously have to be avoided. Because large temperature gradients may yield material stresses and may reduce the life-time of the MCFC considerably or may even lead to a sudden failure.

Numerical simulations show that the new steady state is reached after $t \approx 1000$ ($\approx$3.5 [hours]), if constant boundary conditions are used. This is much too slow for practical operation. A faster approach to the new steady state solution is, however, possible by controlling the boundary conditions at the anode gas inlet as well as the air inlet via time dependent functions.

As it is practically possible to vary some components of the functions $w_{\mathrm{a,in}}$, $\gamma_{\mathrm{a,in}}$, λ_{air}, ϑ_{air}, R_{back} in time, one can achieve an appropriate trade-off of the two contradicting objectives, load changes as fast as possible and solid temperature gradients as small as possible.

Here an appropriate modelling and mathematics can help. Numerical simulations and optimal control of (validated) models based on physical and chemical laws enable forecasts of the behavior of the MCFC without risking the damage of the expensive device. Afterwards, it can be decided if one wants to apply the new control strategy to a real MCFC, or whether model modifications are necessary as, for example, by imposing additional constraints. Of course, it would be desirable to minimize the maximum solid temperature gradient or alternatively to restrict a suitable norm of the temperature gradient by a so-called state variable inequality constraint. However, the complexity of the model allows only a coarse discretization of the highly dimensional and complicated non-linear PDAE system so that reliable approximations of the gradient are not available. Moreover, the consideration of state constraints within optimal control problems of this complexity and type seems to be beyond today's capability of mathematical theory and numerical methods.

Since a load change to a higher cell current yields higher material stresses, the following scenario is analyzed:

The input cell current is prescribed as a discontinuous step function,

$$I_{\mathrm{cell}}(t) = \begin{cases} I_{\mathrm{cell},1} = 0.7 & \text{if} \quad t \le t^\star\,, \\ I_{\mathrm{cell},2} = 0.75 & \text{if} \quad t > t^\star\,. \end{cases} \tag{4.1}$$

Initial conditions (2.12) at $t = 0 \le t^\star$ are given by the stationary solution for constant cell current $I_{\mathrm{cell},1}$.

In order to find a compromise between the two goals, fast load changes and sufficiently low temperature gradients, we suggest the following procedure:

Since the cell voltage U_{cell} reacts very fast and significantly on an abrupt load change of the cell current and, in addition, has only a retarded impact on the slowest, but most important variable concerning material corrosion, the solid temperature ϑ_{s}, a nearly constant cell voltage is a good indicator that the new steady state associated with the new cell current has already been reached sufficiently closely.

Therefore we choose, at first, the following preliminary cost functional for fast load changes:

$$\min\ J_1[u] = \int_{t^\star}^{t_{\mathrm{f}}} L^U \,\mathrm{d}t \text{ with } L^U = \left[U_{\mathrm{cell}}(t) - U_{\mathrm{cell},2}\right]^2,\ U_{\mathrm{cell},2} = 30.788\,. \tag{4.2}$$

Since temperature gradients cannot be computed reliably as already mentioned, we choose as a second preliminary cost functional

$$\min\ J_2[u] = \int_{t^\star}^{t_{\mathrm{f}}} L^\vartheta \,\mathrm{d}t \text{ with } L^\vartheta = \int_\Omega \left[\vartheta_{\mathrm{s}}(\zeta,t) - \vartheta_{\mathrm{s,ref}}\right]^2 \mathrm{d}\zeta\,, \quad \vartheta_{\mathrm{s,ref}} = 3.1\,. \tag{4.3}$$

For the same reasons as we cannot compute temperature gradients, we also cannot reliably compute a maximum norm of the solid temperature difference. Though this would be desirable in order to prevent locally high temperature differences. They may theoretically occur when using the above averaged objective, but actually they do not as the numerical results will show.

Since the solid temperature veers away extremely slowly from the previous steady state after a load change, we need to consider the cost functional (4.3) only in the

final stage of transition to the new steady state. Moreover, all state variables change on different time scales with the molar fractions faster than the solid temperature and the electrical quantities as fastest variables.

This now suggests the following formulation of the optimal control problem which will actually be applied with slight modifications as explained below:

Find an optimal boundary control vector $u : [t^\star, t_\mathrm{f}] \to \mathbb{R}^6$ in such a way that the cost functional

$$J[u] = \int_{t^\star}^{t_\mathrm{f}} [1 - \varepsilon(t)]\, L^U + \varepsilon(t) L^\vartheta \,\mathrm{d}t \tag{4.4}$$

with a given piecewise continuous function $\varepsilon\colon [t^\star, t_\mathrm{f}] \longrightarrow [0,1]$ is minimized subject to the PDAE/integro-DAE (2.1–2.15) and to the set of admissible controls $u(t) \in U \stackrel{\mathrm{def}}{=} \{u \in \mathbb{R}^6 \mid \underline{u}_i \le u_i \le \overline{u}_i, i = 1, \ldots, 6\}$ which is defined in Table 4.1. For the purpose of orientation, the values $u_{i,\mathrm{ref}}$, that have been used for the computation of the steady state solution, are given, too; compare Table 3.1.

TABLE 4.1
Control constraints and reference values

	$\underline{u}_i$	$u_{i,\mathrm{ref}}$	$\overline{u}_i$
$u_1 = \chi_{\mathrm{CH_4,a,in}}$	0.25	2/7	0.35
$u_2 = \gamma_{\mathrm{a,in}}$	0.9	1.0	1.1
$u_3 = \vartheta_{\mathrm{a,in}}$	2.9	3.0	3.1
$u_4 = \lambda_{\mathrm{air}}$	1.8	2.2	2.2
$u_5 = \vartheta_{\mathrm{air}}$	1.3	1.5	1.7
$u_6 = R_{\mathrm{back}}$	0.45	0.5	0.55

Since the molar fraction $\chi_{\mathrm{CH_4,a,in}}$ is chosen as the only boundary control variable, among the molar fractions, at the anode gas inlet, the other molar fractions must fulfill $\chi_{\mathrm{H_2O,a,in}} = 1 - \chi_{\mathrm{CH_4,a,in}}$, $\chi_{k,\mathrm{a,in}} = 0$, $k \notin \{\mathrm{CH_4}, \mathrm{H_2O}\}$.

Because of the aforementioned slow dynamical behavior of the solid temperature, we choose $\varepsilon(t) = 0$ for $t^\star \le t \le t_\mathrm{s}$ and $\varepsilon(t) = 1$ for $t_\mathrm{s} < t \le t_\mathrm{f}$. In order to reduce the runtime for the problem (4.4,2.1–2.15), we split the integral in (4.4) in five segments. Because of the aforementioned different time scales, we introduce heuristically the following logarithmic-type grid $t_1 := t^\star = 0$, $t_2 := 0.1$, $t_3 := 1.1$, $t_4 := 11.1$, $t_5 := t_\mathrm{s} = 111.1$, $t_6 := t_\mathrm{f} = 1111.1$.

This yields the following sequence of optimal control problems

$$\Big(\min \int_{t_k}^{t_{k+1}} L_k \,\mathrm{d}t \;\text{ s.t. (2.1–2.15) and } u(t) \in U\Big)_{k=1,\ldots,5} \tag{4.5}$$

with $L_k := L^U$ for $k = 1, 2, 3, 4$ and $L_5 := L^\vartheta$.

Hereby, the initial conditions for the first optimal control problem of (4.5) is given by the stationary solution for $I_{\mathrm{cell},1}$. The initial conditions for the k-th optimal control problem are then the free final conditions of the $(k-1)$-th optimal control problem. Obviously, this procedure yields only a suboptimal solution. In the present application, this should not have a considerable influence, since no terminal constraints are imposed. This approach is comparable to widely used model predictive control techniques.

Two procedures are common to tackle optimal control problems numerically: *first optimize, then discretize* versus *first discretize, then optimize*. Due to the complexity

of the model and the frequent requirements for model modifications during the project phase, only the latter procedure seems to be applicable.

Hence, we have semi-discretized the PDAE/integro-DAE constraint (2.1–2.15) yielding the semi-explicit DAE (2.16) as mentioned before. The numerical solution of the resulting huge scale DAE-constrained optimal control problem is then computed by the standard software package NUDOCCCS [3]. By means of this package, the infinite dimensional optimal control problem is transformed into a nonlinear programming problem that, at the end, is solved by the sparse SQP method SNOPT [8]. The employment of these approved software modules unfortunately enforces numerical differentiation for the computation of gradient information, which is needed for the optimization, since adjoint information seems to be hardly available. Undoubtedly, automatic differentiation might speed up the runtime here. Another bottleneck is the still rather limited number of variables which can be treated by today's best general purpose NLP software and which restricts the fineness of the discretization drastically.[1]

In order to give more details, each time interval $[t_k, t_{k+1}]$ is partitioned by 21 equidistant nodes for the control grid. The spatial discretization used was usually 10×10. Due to the triple integral in the cost functional (4.5) on $[t_s, t_f]$, we have here used a coarser discretization of 3×3. Nevertheless, the runtime solely for the last optimal control problem on the subinterval $[t_s, t_f]$ is 36 hours.

In the two Figs. 4.1, approximate optimal solutions for the solid temperature ϑ_s at t_f are shown: on the left, $L_5 = L^\vartheta$ has been chosen in the cost functional (4.5), on the right $L_5 = L^U$ has been chosen. One can clearly see the improved profile of the solid temperature ϑ_s in Fig. 4.1 (left) due to the consideration of the two functionals (4.2) and (4.3). The maximum solid temperature is still attained in the corner ($\zeta_1 = 1, \zeta_2 = 1$), but its value has changed from $3.217 \,\widehat{=}\, 959$ [K] to $3.120 \,\widehat{=}\, 930$ [K]. The minimum solid temperature, however, has changed from the corner ($\zeta_1 = 1, \zeta_2 = 0$) to the corner ($\zeta_1 = 0, \zeta_2 = 0$) from $3.090 \,\widehat{=}\, 921$ [K] to $3.021 \,\widehat{=}\, 901$ [K]. The maximum temperature difference could thereby be reduced from $0.196 \,\widehat{=}\, 58$ [K] to $0.023 \,\widehat{=}\, 9$ [K].

Note that the flat solid temperature distribution of Fig. 4.1 (left) can only be obtained by using all six boundary control functions $\chi_{CH_4,a,in}$, $\vartheta_{a,in}$, $\gamma_{a,in}$, λ_{air}, ϑ_{air}, and R_{back}. However, a less flattened solid temperature distribution similar to Fig. 4.1 (right) can almost be achieved by the scalar boundary control $\gamma_{a,in}$ solely. This indicates that this control provides the strongest possibility of exerting an influence. As can be seen, the cell's mild dynamical behavior justifies the poor discretization we were forced to accept due to the various restrictions we have already mentioned.

Additional numerical results for other technologically interesting scenarios can be found in [23].

5. Conclusions. Numerical simulation and optimal control have been performed for a realistic, detailed, highly complex, large scale mathematical model describing the dynamical behavior of a molten carbonate fuel cell. The validation of a closely related model on a real fuel cell and the very similar results of a numerical simulation by finite volume discretization by means of ProMoT/DIVA [16] suggest the reliability of the model and its numerical realisation despite the deficiencies with respect to the resolution of the discretization scheme. Therefore, these simulations and the associated results for the optimally controlled fuel cell (together with the real-time state

[1] The authors have tried to employ also the interior point solver IPOPT [21] via the modelling language AMPL [1] which would enable automatic differentiation, though without success so far.

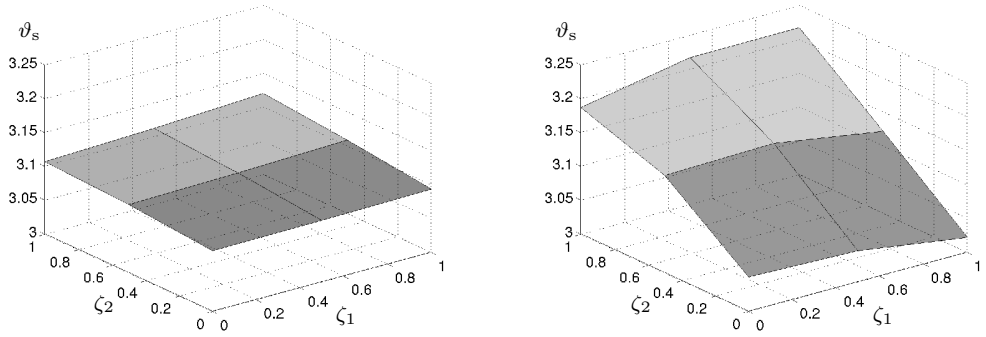

FIG. 4.1. *Solid temperature ϑ_s at time $t_f = 1111.1$ after the load change (4.1) with cost functional $L_5 = L^{\vartheta}$ in $[t_5, t_6]$ (left side) and $L_5 = L^{U}$ in $[t_5, t_6]$ (right side)*

estimator [9]) will certainly lead to a wider range of suitable control strategies for future operations of MCFC.

A comparison of the numerical results for the 1D counterflow model [4] with the 2D crossflow model yields that the 2D solid temperature distribution cannot be predicted by the 1D model. However, the numerical results for the different 2D crossflow models suggest that a detailed modeling of the partial pressures of the gas components in the pores can be neglected. Moreover, a combined chemical equation for the two reforming reactions without considering the carbon monoxide fraction is also meaningful. The resulting deviations are minor; see [23].

Finally, the optimal control results can be further examinated by a numerical sensitivity analysis analogously to [25]. Because of the complexity, the simplifications just suggested should be made when performing a sensitivity analysis.

Due to the enormous computational effort to solve the PDAE/integro DAE system, the application of model reduction techniques, such as, e. g., proper orthogonal decomposition techniques seems to be inevitable; compare [9].

Acknowledgments. We are indebted to Prof. Dr.-Ing. Kai Sundmacher and Dr.-Ing. Peter Heidebrecht from the Max-Planck-Institut für Dynamik komplexer technischer Systeme, Magdeburg, for providing us with the realistic fuel cell models and to Dr.-Ing. h.c. Dipl.-Ing. Joachim F. Berndt and Dipl.-Ing. Mario Koch of the IPF Heizkraftwerksbetriebsgesellschaft mbH, Magdeburg, for their continual support. We are further indebted to Prof. Dr. Christof Büskens from the University of Bremen for making the direct optimal control software package NUDOCCCS available. We also thank Prof. Philip E. Gill from the University of California, San Diego, for the software package SNOPT.

Last but not least the authors would like to thank the anonymous referees for their suggestions, particulary for including the full set of equations. This and their other comments have considerably improved the paper.

Appendix A. Details of the model equations.

A.1. Constants. All constants are summarized in the following tables:

TABLE A.1
Constants

c_p	4.5	F	3.5/8	$\chi_{\mathrm{O_2,air}}$	0.21
$c_\mathrm{p,s}$	10000	κ_e	1	ϑ_u	1
St_as	80.0	c_a	0.00001	κ_1	0.666/2.5,
St_cs	120.0	c_e	0.00001	κ_2	$1/(0.666 \cdot 2.5)$
St_m	1.0	c_c	0.00001	f_blower	0.1

j	Da_j	Arr_j	ϑ_j^0	$\Delta_\mathrm{R}h_j$	α_j^+	α_j^-	n_j
ref1	25.0	84.4	2.93	90.5			
ref2	100.0	6.2	2.93	-14.5			
ox1	5.0	21.6	2.93	56.0	0.5		2
ox2	5.0	21.6	2.93	42.0	0.5		2
red	0.3	31.2	2.93	156.0	2.5	0.5	2

i	$\Delta_\mathrm{C}h_i$	$\nu_{i,\mathrm{ref1}}$	$\nu_{i,\mathrm{ref2}}$	$\nu_{i,\mathrm{ox1}}$	$\nu_{i,\mathrm{ox2}}$	$\nu_{i,\mathrm{red}}$
CH_4	-323.85	-1	0	0	0	0
H_2O	0	-1	-1	1	0	0
H_2	-97.62	3	1	-1	0	0
CO	-114.22	1	-1	0	-1	0
CO_2	0	0	1	1	2	-1
O_2	0	0	0	0	0	-0.5
N_2	0	0	0	0	0	0

k	$\nu_{k,\mathrm{C\ CH_4}}$	$\nu_{k,\mathrm{C\ H_2O}}$	$\nu_{k,\mathrm{C\ H_2}}$	$\nu_{k,\mathrm{C\ CO}}$	$\nu_{k,\mathrm{C\ CO_2}}$	$\nu_{k,\mathrm{C\ O_2}}$	$\nu_{k,\mathrm{C\ N_2}}$
CH_4	-1	0	0	0	0	0	0
H_2O	2	0	1	0	0	0	0
H_2	0	0	-1	0	0	0	0
CO	0	0	0	-1	0	0	0
CO_2	1	0	0	1	0	0	0
O_2	-2	0	-0.5	-0.5	0	0	0
N_2	0	0	0	0	0	0	0

$$\bar{\nu}_j = \sum_{k\in\mathcal{I}} \nu_{k,j}, \quad \bar{\nu}_j^+ = \sum_{k\in\mathcal{I},\nu_{k,j}>0} \nu_{k,j}, \quad \bar{\nu}_j^- = \sum_{k\in\mathcal{I},\nu_{k,j}<0} \nu_{k,j}, \quad \bar{\nu}_{\mathrm{C},j} = \sum_{k\in\mathcal{I}} \nu_{k,\mathrm{C}\ j},$$

$$D_{k,\mathrm{as}} = D_{k,\mathrm{cs}} = 100, \quad k \in \mathcal{I}.$$

A.2. Reaction kinetics. The following quantities describing the reaction kinetics appear in almost all equations.

$$r_\mathrm{ref1} = \exp\left[Arr_\mathrm{ref1}\left(\frac{1}{\vartheta^0_\mathrm{ref1}} - \frac{1}{\vartheta_\mathrm{a}}\right)\right] \cdot \left(\chi_{\mathrm{CH_4,a}}\,\chi_{\mathrm{H_2O,a}} - \frac{\chi^3_{\mathrm{H_2,a}}\,\chi_{\mathrm{CO,a}}}{K_\mathrm{ref1}}\right),$$

$$r_\mathrm{ref2} = \exp\left[Arr_\mathrm{ref2}\left(\frac{1}{\vartheta^0_\mathrm{ref2}} - \frac{1}{\vartheta_\mathrm{a}}\right)\right] \cdot \left(\chi_{\mathrm{CO,a}}\,\chi_{\mathrm{H_2O,a}} - \frac{\chi_{\mathrm{H_2,a}}\,\chi_{\mathrm{CO_2,a}}}{K_\mathrm{ref2}}\right),$$

$$r_{\mathrm{ox1}} = \exp\left[Arr_{\mathrm{ox1}}\left(\frac{1}{\vartheta^0_{\mathrm{ox1}}} - \frac{1}{\vartheta_{\mathrm{s}}}\right)\right]\left\{\varphi_{\mathrm{H_2,a}}\,\exp\left[\frac{\alpha^+_{\mathrm{ox1}}\,n_{\mathrm{ox1}}\,(-\Phi^{\mathrm{L}}_{\mathrm{a}} - \Delta\Phi^0_{\mathrm{ox1}})}{\vartheta_{\mathrm{s}}}\right]\right.$$
$$\left. -\ \varphi_{\mathrm{H_2O,a}}\,\varphi_{\mathrm{CO_2,a}}\,\exp\left[\frac{-(1-\alpha^+_{\mathrm{ox1}})\,n_{\mathrm{ox1}}\,(-\Phi^{\mathrm{L}}_{\mathrm{a}} - \Delta\Phi^0_{\mathrm{ox1}})}{\vartheta_{\mathrm{s}}}\right]\right\},$$
$$r_{\mathrm{ox2}} = \exp\left[Arr_{\mathrm{ox2}}\left(\frac{1}{\vartheta^0_{\mathrm{ox2}}} - \frac{1}{\vartheta_{\mathrm{s}}}\right)\right]\left\{\varphi_{\mathrm{CO,a}}\,\exp\left[\frac{\alpha^+_{\mathrm{ox2}}\,n_{\mathrm{ox2}}\,(-\Phi^{\mathrm{L}}_{\mathrm{a}} - \Delta\Phi^0_{\mathrm{ox2}})}{\vartheta_{\mathrm{s}}}\right]\right.$$
$$\left. -\ \varphi^2_{\mathrm{CO_2,a}}\exp\left[\frac{-(1-\alpha^+_{\mathrm{ox2}})\,n_{\mathrm{ox2}}\,(-\Phi^{\mathrm{L}}_{\mathrm{a}} - \Delta\Phi^0_{\mathrm{ox2}})}{\vartheta_{\mathrm{s}}}\right]\right\},$$
$$r_{\mathrm{red}} = \exp\left[Arr_{\mathrm{red}}\left(\frac{1}{\vartheta^0_{\mathrm{red}}} - \frac{1}{\vartheta_{\mathrm{s}}}\right)\right]\left\{\varphi^{-2}_{\mathrm{CO_2,c}}\,\exp\left[\frac{\alpha^+_{\mathrm{red}}\,(U_{\mathrm{cell}} - \Phi^{\mathrm{L}}_{\mathrm{c}} - \Delta\Phi^0_{\mathrm{red}})}{\vartheta_{\mathrm{s}}}\right]\right.$$
$$\left. -\ \varphi^{0.75}_{\mathrm{O_2,c}}\,\varphi^{-0.5}_{\mathrm{CO_2,c}}\,\exp\left[\frac{-\alpha^-_{\mathrm{red}}\,(U_{\mathrm{cell}} - \Phi^{\mathrm{L}}_{\mathrm{c}} - \Delta\Phi^0_{\mathrm{red}})}{\vartheta_{\mathrm{s}}}\right]\right\};$$

$$K_{\mathrm{ref1}}(\vartheta_{\mathrm{a}}) = \exp(30.19 - 90.41/\vartheta_{\mathrm{a}})\,, \quad K_{\mathrm{ref2}}(\vartheta_{\mathrm{a}}) = \exp(-3.97 + 14.57/\vartheta_{\mathrm{a}})\,,$$
$$\Delta\Phi^0_{\mathrm{ox1}}(\vartheta_{\mathrm{s}}) = 28.26 - 19.84\,\vartheta_{\mathrm{s}}\,, \quad \Delta\Phi^0_{\mathrm{ox2}}(\vartheta_{\mathrm{s}}) = 20.98 - 17.86\,\vartheta_{\mathrm{s}}\,,$$
$$\Delta\Phi^0_{\mathrm{red}}(\vartheta_{\mathrm{s}}) = 78.00 - 23.06\,\vartheta_{\mathrm{s}}\,.$$

A.3. Current densities. With the following abbreviations, the electrical submodel (2.8–2.12) is completed.

$$i_{\mathrm{a}} = F\sum_{j=\mathrm{ox1,ox2}} n_j\,Da_j\,r_j\,, \quad i_{\mathrm{e}} = (\Phi^{\mathrm{L}}_{\mathrm{a}} - \Phi^{\mathrm{L}}_{\mathrm{c}})\,\kappa_{\mathrm{e}}\,, \quad i_{\mathrm{c}} = -\,F\,n_{\mathrm{red}}\,Da_{\mathrm{red}}\,r_{\mathrm{red}}\,.$$

A.4. Heat exchange density. The heat exchange between the gas phases and the solid are modelled by the following functions.

$$q_{\mathrm{as}} = St_{\mathrm{as}}\,(\vartheta_{\mathrm{s}} - \vartheta_{\mathrm{a}})\,, \quad q_{\mathrm{cs}} = St_{\mathrm{cs}}\,(\vartheta_{\mathrm{s}} - \vartheta_{\mathrm{c}})\,,$$
$$q_{\mathrm{solid}} = (\Phi^{\mathrm{L}}_{\mathrm{a}} - \Phi^{\mathrm{L}}_{\mathrm{c}})\,i_{\mathrm{e}}/F - \sum_{j=\mathrm{ox1,2}}\left[\Delta_{\mathrm{R}}h_j + n_j\,\Phi^{\mathrm{L}}_{\mathrm{a}}\right]Da_j\,r_j$$
$$-\left[\Delta_{\mathrm{R}}h_{\mathrm{red}} - n_{\mathrm{red}}\,(U_{\mathrm{cell}} - \Phi^{\mathrm{L}}_{\mathrm{c}})\right]Da_{\mathrm{red}}\,r_{\mathrm{red}}\,.$$

A.5. Heat equation. The source term of the heat equation (2.1) is given by

$$\psi_1 = \Big(-(\vartheta_{\mathrm{c}} - \vartheta_{\mathrm{s}})\,\bar\nu^-_{\mathrm{red}}\,Da_{\mathrm{red}}\,r_{\mathrm{red}} - \sum_{j=\mathrm{ox1,2}}(\vartheta_{\mathrm{a}} - \vartheta_{\mathrm{s}})\,\bar\nu^-_j\,Da_j\,r_j\Big)\,c_{\mathrm{p}}$$
$$+\,q_{\mathrm{solid}} - q_{\mathrm{as}} - q_{\mathrm{cs}}\,.$$

A.6. Hyperbolic transport equations. The systems of hyperbolic equations (2.2, 2.3) for the molar fractions and gas temperatures are given in detail by

$$\frac{\partial\chi_{k,\mathrm{a}}}{\partial t} + \gamma_{\mathrm{a}}\,\vartheta_{\mathrm{a}}\,\frac{\partial\chi_{k,\mathrm{a}}}{\partial\zeta_1} = \vartheta_{\mathrm{a}}\sum_{j=\mathrm{ox1,2,ref1,2}}(\nu_{k,j} - \chi_{k,\mathrm{a}}\,\bar\nu_j)\,Da_j\,r_j\,, \quad k\in\mathcal{I}\,,$$
$$\frac{\partial\chi_{k,\mathrm{c}}}{\partial t} + \gamma_{\mathrm{c}}\,\vartheta_{\mathrm{c}}\,\frac{\partial\chi_{k,\mathrm{c}}}{\partial\zeta_2} = \vartheta_{\mathrm{c}}\,(\nu_{k,\mathrm{red}} - \chi_{k,\mathrm{c}}\,\bar\nu_{\mathrm{red}})\,Da_{\mathrm{red}}\,r_{\mathrm{red}}\,, \quad k\in\mathcal{I}\,,$$

$$\frac{\partial \vartheta_{\mathrm{a}}}{\partial t} + \gamma_{\mathrm{a}}\,\vartheta_{\mathrm{a}}\,\frac{\partial \vartheta_{\mathrm{a}}}{\partial \zeta_1} = \Big(\sum_{j=\mathrm{ref1,2}} -\Delta_{\mathrm{R}} h_j\, Da_j\, r_j + \sum_{j=\mathrm{ox1,2}} \bar{\nu}_j\, Da_j\, r_j\, (\vartheta_{\mathrm{s}} - \vartheta_{\mathrm{a}})\, c_{\mathrm{p}} + q_{\mathrm{as}} \Big)\, \frac{\vartheta_{\mathrm{a}}}{c_{\mathrm{p}}}\,,$$

$$\frac{\partial \vartheta_{\mathrm{c}}}{\partial t} + \gamma_{\mathrm{c}}\,\vartheta_{\mathrm{c}}\,\frac{\partial \vartheta_{\mathrm{c}}}{\partial \zeta_2} = \vartheta_{\mathrm{c}}\,\bar{\nu}^{-}_{\mathrm{red}}\, Da_{\mathrm{red}}\, r_{\mathrm{red}}\, (\vartheta_{\mathrm{s}} - \vartheta_{\mathrm{c}}) + \frac{\vartheta_{\mathrm{c}}\, q_{\mathrm{cs}}}{c_{\mathrm{p}}}\,.$$

The degenerate equations (2.4, 2.5) for the molar flow densities are given by

$$\frac{\partial(\gamma_{\mathrm{a}}\,\vartheta_{\mathrm{a}})}{\partial \zeta_1} = \sum_{j=\mathrm{ref1,2}} -\Delta_{\mathrm{R}} h_j\, Da_j\, r_j / c_{\mathrm{p}} + \sum_{j=\mathrm{ox1,2}} \bar{\nu}^{+}_j\, Da_j\, r_j\, (\vartheta_{\mathrm{s}} - \vartheta_{\mathrm{a}}) + \frac{q_{\mathrm{as}}}{c_{\mathrm{p}}} + \vartheta_{\mathrm{a}} \sum_{j=\mathrm{ox1,2,ref1,2}} \bar{\nu}_j\, Da_j\, r_j\,,$$

$$\frac{\partial(\gamma_{\mathrm{c}}\,\vartheta_{\mathrm{c}})}{\partial \zeta_2} = \vartheta_{\mathrm{c}}\,\bar{\nu}_{\mathrm{red}}\, Da_{\mathrm{red}}\, r_{\mathrm{red}} + \vartheta_{\mathrm{c}}\,\bar{\nu}^{-}_{\mathrm{red}}\, Da_{\mathrm{red}}\, r_{\mathrm{red}}\, (\vartheta_{\mathrm{s}} - \vartheta_{\mathrm{c}}) + \frac{q_{\mathrm{cs}}}{c_{\mathrm{p}}}\,.$$

A.7. Pores. The systems of algebraic equations (2.6) for the partial pressures in the pores are given by

$$0 = \sum_{j=\mathrm{ox1,2}} \nu_{k,j}\, Da_j\, r_j - D_{k,\mathrm{as}}\, (\varphi_{k,\mathrm{a}} - \chi_{k,\mathrm{a}}), \quad k \in \mathcal{I}\,,$$

$$0 = \sum_{j=\mathrm{red}} \nu_{k,j}\, Da_j\, r_j - D_{k,\mathrm{cs}}\, (\varphi_{k,\mathrm{c}} - \chi_{k,\mathrm{c}}), \quad k \in \mathcal{I}\,.$$

A.8. Catalytic burner and mixer. A detailed exposition of the equations (2.13, 2.14), which couple, on the one hand, the anode outlet with the cathode inlet via the catalytic burner with its associated air inlet and the mixer, and, on the other hand, the cathode outlet with the catalytic burner via the recycle are given subsequently.

A.8.1. Spatial averages at anode outlet.

$$\gamma_{\mathrm{a,out}}(t) := \int_0^1 \gamma_{\mathrm{a}}(\zeta_1 = 1, \zeta_2, t)\ \mathrm{d}\zeta_2\,,$$

$$\chi_{k,\mathrm{a,out}}(t) := \frac{1}{\gamma_{\mathrm{a,out}}(t)} \int_0^1 \gamma_{\mathrm{a}}(\zeta_1 = 1, \zeta_2, t)\, \chi_{k,\mathrm{a}}(\zeta_1 = 1, \zeta_2, t)\ \mathrm{d}\zeta_2\,, \quad k \in \mathcal{I}\,,$$

$$\vartheta_{\mathrm{a,out}}(t) := \frac{1}{\gamma_{\mathrm{a,out}}(t)} \int_0^1 \gamma_{\mathrm{a}}(\zeta_1 = 1, \zeta_2, t)\, \vartheta_{\mathrm{a}}(\zeta_1 = 1, \zeta_2, t)\ \mathrm{d}\zeta_2\,.$$

A.8.2. Spatial averages at cathode outlet.

$$\gamma_{\mathrm{c,out}}(t) := \int_0^1 \gamma_{\mathrm{c}}(\zeta_1, \zeta_2 = 1, t)\ \mathrm{d}\zeta_1\,,$$

$$\chi_{k,\mathrm{c,out}}(t) := \frac{1}{\gamma_{\mathrm{c,out}}(t)} \int_0^1 \gamma_{\mathrm{c}}(\zeta_1, \zeta_2 = 1, t)\, \chi_{k,\mathrm{c}}(\zeta_1, \zeta_2 = 1, t)\ \mathrm{d}\zeta_1\,, \quad k \in \mathcal{I}\,,$$

$$\vartheta_{\mathrm{c,out}}(t) := \frac{1}{\gamma_{\mathrm{c,out}}(t)} \int_0^1 \gamma_{\mathrm{c}}(\zeta_1, \zeta_2 = 1, t)\, \vartheta_{\mathrm{c}}(\zeta_1, \zeta_2 = 1, t)\ \mathrm{d}\zeta_1\,.$$

A.8.3. Catalytic burner.

$$\chi_{O_2,\mathrm{air}} = 0.21, \quad \chi_{N_2,\mathrm{air}} = 1 - \chi_{O_2,\mathrm{air}}, \quad \chi_{k,\mathrm{air}} = 0, \quad k \notin \{O_2, N_2\}\,,$$

$$\begin{aligned}
\gamma_{\mathrm{b}}(t) &= \gamma_{\mathrm{a,out}}(t)\,\Big(1 + \sum_{k\in\mathcal{I}} \bar{\nu}_{\mathrm{C},k}\,\chi_{k,\mathrm{a,out}}(t)\Big) \\
&\quad + \gamma_{\mathrm{c,out}}(t)\,R_{\mathrm{back}}(t)\Big(1 + \sum_{k\in\mathcal{I}} \bar{\nu}_{\mathrm{C},k}\,\chi_{k,\mathrm{c,out}}(t)\Big) \\
&\quad + \gamma_{\mathrm{air}}(t)\,\Big(1 + \sum_{k\in\mathcal{I}} \bar{\nu}_{\mathrm{C},k}\,\chi_{k,\mathrm{air}}(t)\Big)\,, \\
\gamma_{\mathrm{air}}(t) &= \gamma_{\mathrm{a,in}}(t)\,\frac{\lambda_{\mathrm{air}}(t)}{\chi_{O_2,\mathrm{air}}(t)}\,\Big(-\chi_{O_2,\mathrm{a,in}}(t) - \sum_{k\in\mathcal{I}} \nu_{O_2,\mathrm{C}k}\,\chi_{k,\mathrm{a,in}}(t)\Big)\,, \\
\chi_{k,\mathrm{b}}(t) &= \frac{\gamma_{\mathrm{a,out}}(t)}{\gamma_{\mathrm{b}}(t)}\,\Big(\chi_{k,\mathrm{a,out}}(t) + \sum_{j\in\mathcal{I}} \nu_{k,\mathrm{C}j}\,\chi_{j,\mathrm{a,out}}(t)\Big) \\
&\quad + \frac{\gamma_{\mathrm{c,out}}(t)\,R_{\mathrm{back}}(t)}{\gamma_{\mathrm{b}}(t)}\,\Big(\chi_{k,\mathrm{c,out}}(t) + \sum_{j\in\mathcal{I}} \nu_{k,\mathrm{C}j}\,\chi_{j,\mathrm{c,out}}(t)\Big) \\
&\quad + \frac{\gamma_{\mathrm{air}}(t)}{\gamma_{\mathrm{b}}(t)}\,\Big(\chi_{k,\mathrm{air}}(t) + \sum_{j\in\mathcal{I}} \nu_{k,\mathrm{C}j}\,\chi_{j,\mathrm{air}}(t)\Big)\,, \quad k \in \mathcal{I}\,, \\
\vartheta_{\mathrm{b}}(t) &= \frac{\gamma_{\mathrm{c,out}}(t)\,R_{\mathrm{back}}(t)}{\gamma_{\mathrm{b}}(t)\,c_{\mathrm{p}}}\,\Big(c_{\mathrm{p}}\;(\vartheta_{\mathrm{a,out}}(t) - 1) - \sum_{k\in\mathcal{I}} \chi_{k,\mathrm{a,out}}(t)\,\Delta_{\mathrm{C}}h_k\Big) \\
&\quad + \frac{\gamma_{\mathrm{c,out}}(t)\,R_{\mathrm{back}}(t)}{\gamma_{\mathrm{b}}(t)\,c_{\mathrm{p}}}\Big(c_{\mathrm{p}}\;(\vartheta_{\mathrm{c,out}}(t) - 1) - \sum_{k\in\mathcal{I}} \chi_{k,\mathrm{c,out}}(t)\,\Delta_{\mathrm{C}}h_k\Big) \\
&\quad + \frac{\gamma_{\mathrm{air}}(t)}{\gamma_{\mathrm{b}}(t)\,c_{\mathrm{p}}}\Big(c_{\mathrm{p}}\;(\vartheta_{\mathrm{air}}(t) - 1) - \sum_{k\in\mathcal{I}} \chi_{k,\mathrm{air}}(t)\,\Delta_{\mathrm{C}}h_k\Big)\,.
\end{aligned}$$

A.8.4. Mixer.

$$\begin{aligned}
Q_{\mathrm{m}} &= St_{\mathrm{m}}\,(\vartheta_{\mathrm{m}} - \vartheta_{\mathrm{u}})\,, \\
\frac{\mathrm{d}\chi_{k,\mathrm{m}}}{\mathrm{d}t} &= \gamma_{\mathrm{b}}(t)\,\big(\chi_{k,\mathrm{b}}(t) - \chi_{k,\mathrm{m}}(t)\big)\,\frac{\vartheta_{\mathrm{m}}(t)}{5}\,, \quad k \in \mathcal{I}\,, \\
\frac{\mathrm{d}\vartheta_{\mathrm{m}}}{\mathrm{d}t} &= \gamma_{\mathrm{b}}(t)\,\big(\vartheta_{\mathrm{b}}(t) - \vartheta_{\mathrm{m}}(t)\big)\,\frac{\vartheta_{\mathrm{m}}(t)}{5} - \frac{Q_{\mathrm{m}}}{c_{\mathrm{p}}}\,\frac{\vartheta_{\mathrm{m}}(t)}{5}\,, \\
\gamma_{\mathrm{m}}(t) &= \gamma_{\mathrm{b}}(t)\,\frac{\vartheta_{\mathrm{b}}(t)}{\vartheta_{\mathrm{m}}(t)} - \frac{Q_{\mathrm{m}}}{c_{\mathrm{p}}\,\vartheta_{\mathrm{m}}(t)}\,.
\end{aligned}$$

REFERENCES

[1] The AMPL Company, `http://www.ampl.com/`, 2007.

[2] M. Bischoff and G. Huppmann, *Operating Experience with a 250 kW_{el} Molten Carbonate Fuel Cell (MCFC) Power Plant,* Journal of Power Sources 105, 2 (2002), 216–221.

[3] C. Büskens, *Optimierungsmethoden und Sensitivitätsanalyse für optimale Steuerprozesse mit Steuer- und Zustands-Beschränkungen,* Dissertation, Universität Münster, Germany, 1998.

[4] K. Chudej, M. Bauer, H. J. Pesch, and K. Schittkowski, *Numerical Simulation of a Molten Carbonate Fuel Cell by Partial Differential Algebraic Equations,* in "From Nano to Space,

Applied Mathematics Inspired by Roland Bulirsch", M. Breitner, G. Denk, P. Rentrop, eds., Springer, Berlin, 2008, 57–70.

[5] K. Chudej, P. Heidebrecht, V. Petzet, S. Scherdel, K. Schittkowski, H. J. Pesch, and K. Sundmacher, *Index Analysis and Numerical Solution of a Large Scale Nonlinear PDAE System Describing the Dynamical Behaviour of Molten Carbonate Fuel Cells,* Z. angew. Math. Mech. 85 (2005), 132–140.

[6] K. Chudej, H. J. Pesch, and J. Rang, *Index Analysis of Models*, in [26], 2007, 63–74.

[7] K. Chudej, K. Sternberg, and H. J. Pesch, *Simulation and Optimal Control of Molten Carbonate Fuel Cells,* in Proceedings 5th MATHMOD Vienna, I. Troch, F. Breitenecker, eds., Argesim-Verlag, Wien, Austria, Report No 30, 2006.

[8] P. E. Gill, W. Murray, and M. A. Saunders, *SNOPT: An SQP Algorithm for Large-scale Constrained Optimization*, Numerical Analysis Report 97-1, Department of Mathematics, University of California, San Diego, La Jolla, CA, 1997.

[9] M. Grötsch, M. Mangold, M. Sheng, and A. Kienle, *Model Reduction and State Estimation,* in [26], 2007, 185–200.

[10] M. Gundermann, P. Heidebrecht, and K. Sundmacher, *Validation of a Mathematical Model Using an Industrial MCFC Plant,* ASME J. Fuel Cell Sci. Technol. 3 (2006), 303–307.

[11] P. Heidebrecht, *Modelling, Analysis and Optimisation of a Molten Carbonate Fuel Cell with Direct Internal Reforming (DIR-MCFC)*, VDI Fortschritt-Berichte, Reihe 3, Nr. 826, VDI Verlag, Düsseldorf, Germany, 2005. (ISBN 3183826038)

[12] P. Heidebrecht and K. Sundmacher, *Dynamic Modeling and Simulation of a Counter Flow Molten Carbonate Fuel Cell (MCFC) with Internal Reforming,* Fuel Cells 3–4 (2002), 166–180.

[13] P. Heidebrecht and K. Sundmacher, *Dynamic Model of a Cross-Flow Molten Carbonate Fuel Cell with Direct Internal Reforming*, Journal of the Electrochemical Society 152 (2005), A2217–A2228.

[14] P. Heidebrecht and K. Sundmacher, *Conceptual Design of the Integration of the Reforming Process in High Temperature Fuel Cells*, Journal of Power Sources 145 (2005), 40–49.

[15] P. Heidebrecht and K. Sundmacher, *Optimization of Reforming Catalyst Distribution in a Cross-Flow Molten Carbonate Fuel Cell with Direct Internal Reforming*, Ind. Eng. Chem. Res. 44 (2005), 3522–3528.

[16] P. Heidebrecht, M. Gundermann, and K. Sundmacher, *Steady State and Dynamic Process Analysis*, in [26], 2007, 125–140.

[17] P. Heidebrecht, and K. Sundmacher, *MCFC Reference Model*, in [26], 2007, 35–62.

[18] G. Huppmann, *MTU's Carbonate Fuel Cell HotModule*, in [26], 2007, 3–26.

[19] M. Koch, J. F. Berndt, and M. Gundermann, *Operational Experiences*, in [26], 2007, 27–32.

[20] R. Köhler, K. Mohl, H. Schramm, M. Zeitz, M. Mangold, E. Stein, and E. . Gilles, *Method of Lines within the Simulation Enviroment DIVA for Chemical Processes*, in *Adaptive Method of Lines*, A. Vande Wouver, P. Saucez, and W. Schiesser, eds., Chapman & Hall/CRC, Boca Raton, Florida, 2001, 371–406.

[21] C. Laird and A. Wächter, `www.coin-or.org/Ipopt/`; for a documentation including a bibliography see `www.coin-or.org/Ipopt/documentation/`, 2007.

[22] S. Rolf, *Betriebserfahrungen mit dem MTU Hot Module,* in Stationäre Brennstoffzellenanlagen, Markteinführung, VDI Berichte, Nr. 1596, VDI Verlag, Düsseldorf, Germany, 2001, 49–57.

[23] K. Sternberg, *Simulation, Optimale Steuerung und Sensitivitätsanalyse einer Schmelzcarbonat-Brennstoffzelle,* Dissertation, Fakultät für Mathematik und Physik, Universität Bayreuth, Germany, 2007. (http://deposit.ddb.de/cgi-bin/dokserv?idn=984603921)

[24] K. Sternberg, K. Chudej, and H. J. Pesch, *Suboptimal Control of a 2D Molten Carbonate Fuel Cell PDAE Model,* Math. Comput. Model. Dyn. Syst. 13, 5 (2007), 471–485.

[25] K. Sternberg, K. Chudej, H. J. Pesch, and A. Rund *Parametric Sensitivity Analysis of Fast Load Changes of a Dynamic MCFC Model,* ASME J. Fuel Cell Sci. Technol. 5 (2008)

[26] K. Sundmacher, A. Kienle, H. J. Pesch, J. F. Berndt, and G. Huppmann, *Molten Carbonate Fuel Cells – Modeling, Analysis, Simulation, and Control.* Wiley-VCH, Weinheim, Germany, 2007. (ISBN 9783527314744)

[27] T. Tränkle, M. Zeitz, M. Ginkel, and E. D. Gilles, *PROMOT: A Modeling Tool for Chemical Processes,* Math. Comput. Model. Dyn. Syst. 6, 3 (2000), 283–307.

[28] W. Winkler, *Brennstoffzellenanlagen,* Springer, Berlin, Germany, 2002.